Communication

Advances in the Production of PBCA Microparticles Using a Micromixer with HH-Geometry in a Microfluidic System

Aline Rocha Vieira [1,2], Aline Furtado Oliveira [2], Fabiana Vieira Lima Solino Pessoa [3], Beatriz Nogueira Messias de Miranda [2] and André Rolim Baby [1,*]

1   Department of Pharmacy, Faculty of Pharmaceutical Sciences, University of São Paulo, São Paulo 05508-900, Brazil; alinerocha07@usp.br
2   Micromanufacturing Laboratory, Center for Bionanomanufacturing, Institute for Technological Research, São Paulo 05508-901, Brazil
3   Department of Health Sciences, Faculty of Pharmacy, Federal University of Espírito Santo, São Mateus 29932-540, Brazil
*   Correspondence: andrerb@usp.br

Abstract: Different reaction control methods for producing nano/microstructures of poly(butyl cyanoacrylate) (PBCA) have been studied, focusing on pH and monomer-to-initiator ratios. However, these methods often require multiple steps and reagents. In the synthesis of PBCA microparticles using three versions of micromixers designed with HH geometry and varying numbers of channels (4, 10, and 15), different synthesis formulations were investigated by varying monomer concentrations. PBCA microparticles synthesized with 19.2% (w/w) n-butyl cyanoacrylate (n-BCA) monomer, a residence time of 0.06 s, a flow rate of 78 mL·min^{-1}, and a phase ratio of 45/55 (W/O), exhibited an average diameter of 642.2 nm as determined by dynamic light scattering (DLS) analysis. In contrast, PBCA microparticles synthesized with 5.0% (w/w) n-BCA monomer, the same residence time of 0.06 s, a flow rate of 39 mL·min^{-1}, and a phase ratio of 20/80 (W/O), exhibited an average diameter of 74.73 μm according to laser diffraction particle size analysis. Polymer formation was confirmed by Fourier-transform infrared (FTIR) spectroscopy in both formulation and process conditions. These results indicate that the parameters for the production of microparticles with different monomer concentrations in the microfluidic system with HH geometry and 15 channels can be optimized for potential applications in cosmetics and pharmaceutical ingredients.

Keywords: microparticles; PBCA; microfluidic system; geometry HH; micromixer

1. Introduction

Microencapsulation has gained prominence as a technology possessing various advantages, given that it not only increases stability but can also promote the controlled release of these active ingredients and ensure safety in transdermal administration on the skin [1]. The literature documents the use of various materials, including polymers, liposomes, proteins, and polysaccharides, characterized by specific physicochemical and mechanical properties. When microstructured, these materials can mitigate the impact of external factors through the employment of delivery systems as carriers, a strategy long utilized in the cosmetic industry [2]. Microparticles and microspheres are micrometer-scale particles (1–1000 μm in diameter) composed of a polymeric material, also known as the shell material, which encapsulates the active ingredient, referred to as the core. This core can consist of liquids, solids, or gases and may be mononuclear, multinuclear, or matrix-structured [1,3].

Different methods are used for microencapsulation through chemical processes, including emulsion polymerization, suspension polymerization, and interfacial polymerization, among others. The microencapsulation process is not uniform across all materials and applications. The selection of the most suitable technique depends on various factors, including the application of the microsystem, the required particle size, the physical and chemical

properties of the core, the properties of the shell material, the desired controlled release mechanism, and other relevant parameters. Therefore, to produce an encapsulated product, it is essential to consider and combine all these formulations and process characteristics [1].

Interfacial polymerization involves highly reactive monomers or monomers and initiators/catalysts dissolved into two immiscible solvents. When these solutions come into contact, polymerization occurs at the interface. This polymerization reaction is controlled by chemical kinetics, through direct contact with the monomers [4]. The polymer formation occurs due to the rapid polymerization, given the low solubility between phases. During the reaction of the monomers, two solutions diffuse towards the already formed polymer at the interface, resulting in an increase in the thickness of the interfacial film. This increased thickness creates a barrier that hinders further diffusion. The thickness of the film can vary depending on the availability of monomers for the reaction [4–6].

Several factors can influence the polymerization process such as the solubility of the phases, the concentration of the monomers and initiator, the reactivity of the monomers, the solvents, the additives, and the temperature [4–6]. The polymerization procedure occurring during the miniemulsion process is well-suited for the formation of nanocapsules. The choice of monomers/polymers and their specific chemical reactions favors the formation of nanocapsules with either hydrophobic or hydrophilic cores. This technique enables the production of capsules with tailored properties, suitable for a wide range of applications [7,8].

Addition polymerization occurs through the reaction of monomer and the reactive site on the chain growth of the polymer when new monomers are added. The addition of a unit of monomer to the growing chain regenerates the reactive site and the process of polymerization continues repeatedly. Monomers with double or triple bonds are used in addition polymerization [9,10]. The addition polymerization reaction takes place in three steps. During the step of chain initiation, the polymerization reaction is usually started when an initiator creates a reactive site. This initiator can be a cation (cationic polymerization), an anion (anionic polymerization), a radical (free radical polymerization), and an organometallic complex (coordination polymerization) [9,10]. During the chain propagation step, the link between the monomers or repeating units and the molecular chain occurs, increasing the length of the chain. Finally, during the chain termination stage, the chain's growth stops due to the neutralizing of the reactive center [9,10].

Anionic polymerization involves an active center that carries a negative ion (anion), so the chain reaction occurs through an anionic reaction. Anionic polymerization happens quickly, and the polymerization of its termination stage cannot occur through direct combination, but does so through disproportion, by the addition of other reagents to end the chain growth process and control the average molecular weight [9,11]. Generally, ion chain repetition structures have high reactivity, and the ability to combine even at low temperatures and pressures. The polymerization process speed provides for the formation of linear polymer chains [9,11]. Among the materials for the preparation of polymeric nanocarriers, n-butyl cyanoacrylate (n-BCA) is a low-toxic monomer that due to its biodegradability has been one of the most studied materials in the class of alkyl cyanoacrylate [12]. n-BCA has high reactivity and when the polymerization process forms PBCA [13–15].

Among the various areas for its application, PBCA is used to encapsulate pharmaceuticals, bioactive agents, and agents with antibacterial action, among others. The formation of PBCA may occur through different routes, either by miniemulsion [16], interfacial [16,17], or anionic polymerization [17,18]. These mechanisms are derived from polymerization by addition and the polymerization process follows the steps of initiation, reversible propagation, and reversible termination (Figure 1) [12,19,20]. Recently, studies have shown that molar masses below 10,000 g·mol^{-1} can be obtained by anionic polymerization in a miniemulsion, which indicates that this route can help control the reaction, although the pH variation can increase the molecular weight or favor the agglomeration of the nanoparticles [12].
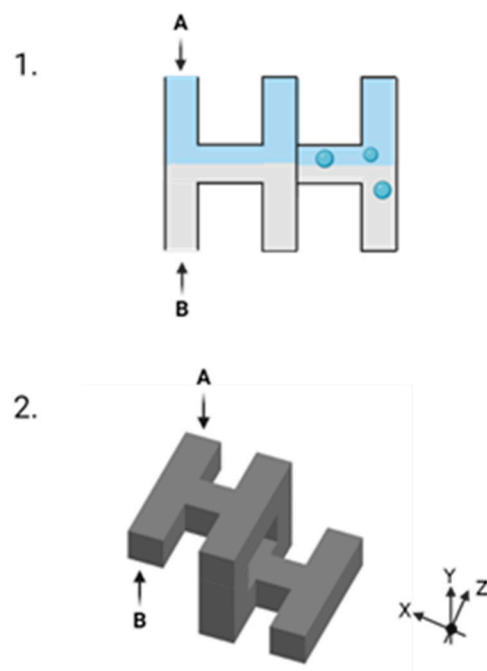
Figure 1. Design of two H segments which constitute the HH geometry micromixer, indicating the inlets for the aqueous phase (A) and the oil phase (B). Legend: 1. 2D scheme of the initial flow within the H-segment; 2. 3D scheme of the H-segment. Sources: Biorender and AutoCAD, the author herself.

Musyanovych and Landfester obtained PCBA nanocapsules containing DNA attained by the anionic polymerization process in a two-stage miniemulsion which was prepared by ultrasonication with pH 7.4 buffered followed by the addition of n-BCA dropwise. They noted that adding the monomer slowly allowed the polymerization to occur at the interface of droplets formed by the PBCA shell. In addition, they reported that the use of surfactant in high concentration contributed to the formation of shorter chains [21]. Hansali and collaborators also used the anionic polymerization process in miniemulsion, although some parameters differed from those of the authors mentioned above. The polymerization took place by the phase inversion process in pH 2 (to achieve emulsification control before starting the polymerization step) with the addition of the aqueous phase using a metering pump drop by drop, and the NaOH solution was added to start the polymerization. The results show that the increase in the water addition rate influenced the size of the particle diameter [22]. Duan and collaborators conducted a co-encapsulation study of doxorubicin hydrochloride (hydrophilic) and hydrophobic curcumin in PBCA nanoparticles using emulsion polymerization for the interfacial polymerization process. Doxorubicin hydrochloride was added directly to the aqueous phase and curcumin to the alcohol solution 10 min after the beginning of the polymerization process. The authors indicated that this was meant to co-encapsulate both assets in a single system [17]. Microfluidics has stood out for its diversity of applications in pharmaceutical, chemical, and analytical chemistry, as well as biochemical analyses and others.

Microfluidic devices are not a miniature version of a process on a macro scale since many physical characteristics can be different, such as surface tension and diffusion, and the surface area/volume ratio does not simply follow a large linear scale for small devices [23–26]. In addition, the presence of laminar flow conditions may vary according to the structure of the device, from the size of fluid passage channels to its geometry. Microfluidic methods can be divided into monophasic continuous (mixture of one or more miscible solvents and components by diffusion in laminar flow) and segmented multiphase flow (interaction between two immiscible fluids, being these divided in a continuous phase and a dispersed phase) [23–28].

The behavior of these fluids in microfluidic channels is characterized by the dimensionless Reynolds number (Re), which provides a quantitative estimate of the likelihood of the fluid developing turbulence. The Re number is calculated using the relationship between the kinematic viscosity, the actual speed of the fluid, and the diameter of the channel, represented by the volume-area relationship [24,29]. Microfluidic systems are generally designed on a microscale to form mixtures using a micromixer and provide the interaction between components according to chemical reactions. Different types of micromixers are studied considering the characteristics of the reactions involved in the process [23,24,27].

Micromixers are divided into two categories: active and passive. In active micromixers, flow disturbances are created through interactions with external energy sources such as electric and magnetic fields or ultrasonic vibrations. In contrast, passive micromixers rely on the pumping of fluids within the micromixer, where mixing occurs through molecular diffusion and chaotic advection [24,27,30].

The geometry of passive micromixers is designed to increase the surface area between different fluids and enhance chaotic advection, while also reducing the diffusion path. Passive micromixers are classified based on their structural dimensions into two-dimensional (2D) and three-dimensional (3D) types. Common structural designs include serpentine, T-type, and zigzag configurations, among others [24,27,30]. When compared, passive 2D and 3D micromixers differ in mixing performance and surface area extension, both of which are better in 3D micromixers, although these models are more complex to manufacture than the 2D ones [30].

Division and recombination (SAR) are described as a typical mixing mechanism, also known as a sequential lamination micromixer. The sequential process in micromixers occurs through the steps of flow division, flow recombination, and flow rearrangement, throughout which the exponential increase in the fluid interface area reduces the path length and improves the mixture favoring speed and its homogeneity [24,30].

Currently, studies that report the usage of 3D serpentine/SAR structures are focused on the process of nanoprecipitation of polymers such as polycaprolactone (PCL) [31], and poly (D, L lactic-co-glycolic) (PLGA) [32,33]. Low-temperature co-fired ceramics (LTCC) are described in the literature as an adequate option for microfluidic devices as they show several advantages compared to other microfabrication technologies. The tapes are composed of vitroceramics, a glass frit binder that helps to reduce the processing temperature [34,35]. The possibility of making 3D structures using several layers of green ribbons is a characteristic of the utmost importance and the microfabrication of these ribbons follows three steps: standardization of the individual layers with all the details according to their usage needs; lamination of tapes under pressure and temperature and lastly sintering of laminated material [34,35].

Finally, in this research, we aimed to evaluate the impacts of the HH geometry micromixer manufactured in LTCC and used in a microfluidic system focusing on the formation of PBCA microparticles without the use of termination reagents through an anionic polymerization reaction in emulsion.

## 2. Materials and Methods

2.1. Materials

The following starting materials were used in this investigation: ethyl alcohol P.A (Química Moderna, São Paulo, Brazil), n-butyl cyanoacrylate (n-BCA) (Evobond, TongShen Enterprise CO., LTD, Taiwan), sorbitan monooleate (Span 80) (Croda, Campinas, Brazil), and caprylic/capric triglycerides (TGCC) (Mapric, São Paulo, Brazil).

2.2. Microfluidic System

2.2.1. Geometry HH

The geometry of the HH micromixer is given based on the SAR process, in which two fluids are mixed, then divided, and recombined during the diffusion process of the mixture. The HH micromixer geometry consists of an H-shaped segment, with each end

of its structure connected to another H-shaped segment. The flow follows a 3D path [36]. The HH geometry was designed based on the model proposed elsewhere [36,37]. The micromixer geometry dimensions have a height of 630 μm and a width of 675 μm, with a hydraulic diameter of 652 μm and a volume of 47.65 mm^3 in the 4-channel micromixer; the 10-channel micromixer has a height of 600 μm and width of 600 μm, with a hydraulic diameter of 1500 μm and a volume of 72.6 mm^3; finally, the 15-channel micromixer has a height of 600 μm and width of 600 μm, with a hydraulic diameter of 2250 μm and a volume of 100.15 mm^3. The geometries were designed as having two inputs and one output (Figure 2).
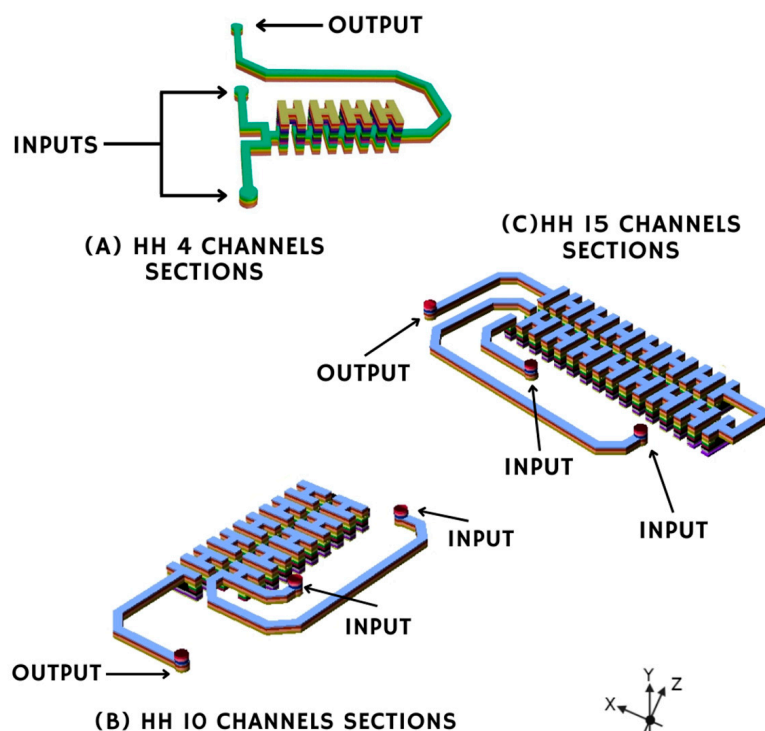

Figure 2. Design of micromixers containing 4, 10, and 15 channels with HH geometry, featuring two inlets and one outlet for each micromixer. Legend: (A). Micromixer containing 4 channels; (B). Micromixer containing 10 channels; and (C). Micromixer containing 15 channels. Both the inlet and outlet of the micromixer are indicated by the arrow. Sources: (Autocad), author herself.

2.2.2. Fabrication of the Microfluidic Device

The microfluidic device was manufactured through a process that included layer cutting, thick film deposition, lamination, sintering, and dicing (Figure 3). Layers with microchannel geometries were fabricated using a diode-pumped IR laser, model U-15 1064 nm Ultrafast Laser Maker (RMI Laser, LLC, Lafayette, CO, USA), and a prototyping machine equipped with an UV laser (length of 355 nm), LPKF Protolaser® U3 (LPKF Laser & Electronics AG, Garbsen, Germany) [31]. The thermocompression lamination process was conducted using a uniaxial laminator under specific conditions. A sequential lamination scheme was employed, utilizing 11.8 MPa of pressure at 70 °C with a hydraulic press (model MA098/A30, Marconi, Piracicaba, São Paulo, Brazil). The lamination procedure lasted 20 min, involving rotation of the device by 90 degrees after the initial 10 min, followed by another 10 min of lamination. In this sequential lamination approach, layers with identical microchannel cut designs were laminated together to form individual blocks. Subsequently, all these blocks were laminated together to produce the final integrated device [31].
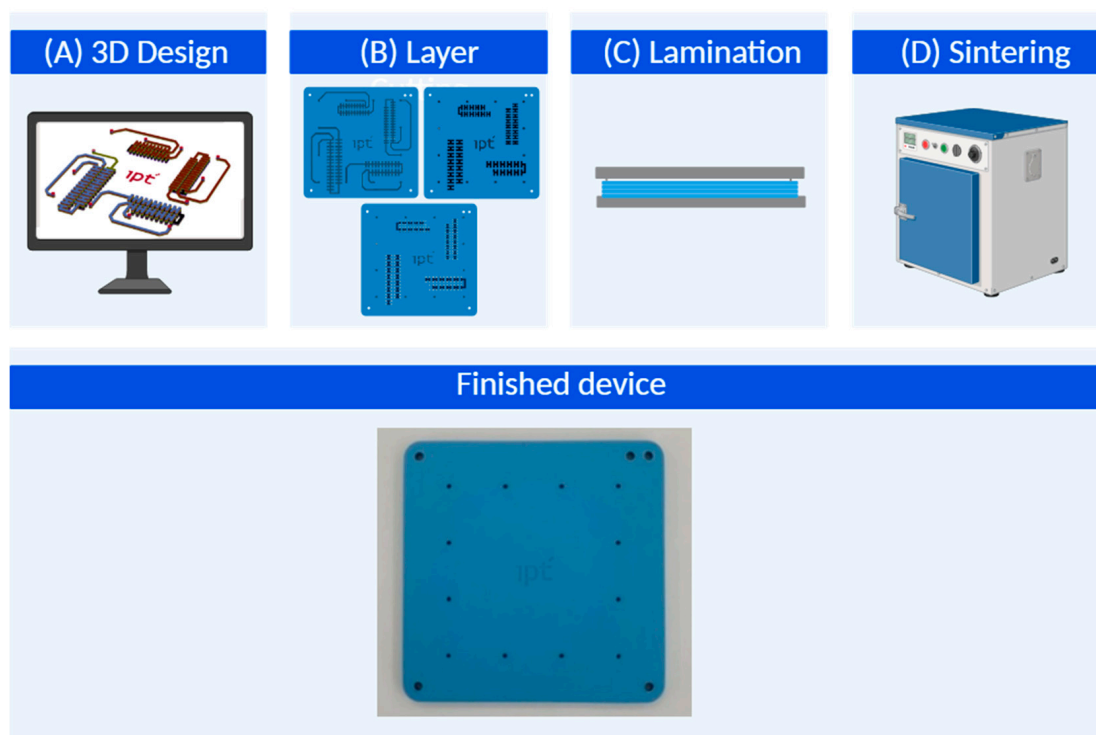
Figure 3. Microfluidic device fabrication steps and microfluidic device fabricated in LTCC. Sources: Biorender, author herself.

2.2.3. Microfluidic System

The microfluidic system was composed of two high-pressure dual-piston pumps (HF Series Pump—SSI, PA, USA), one for continuous phase (oil) feeding and the other for dispersed phase (aqueous) feeding. The microfluidic device containing the micromixer is attached to the manifold, which has two inputs and one output (Figure 4).
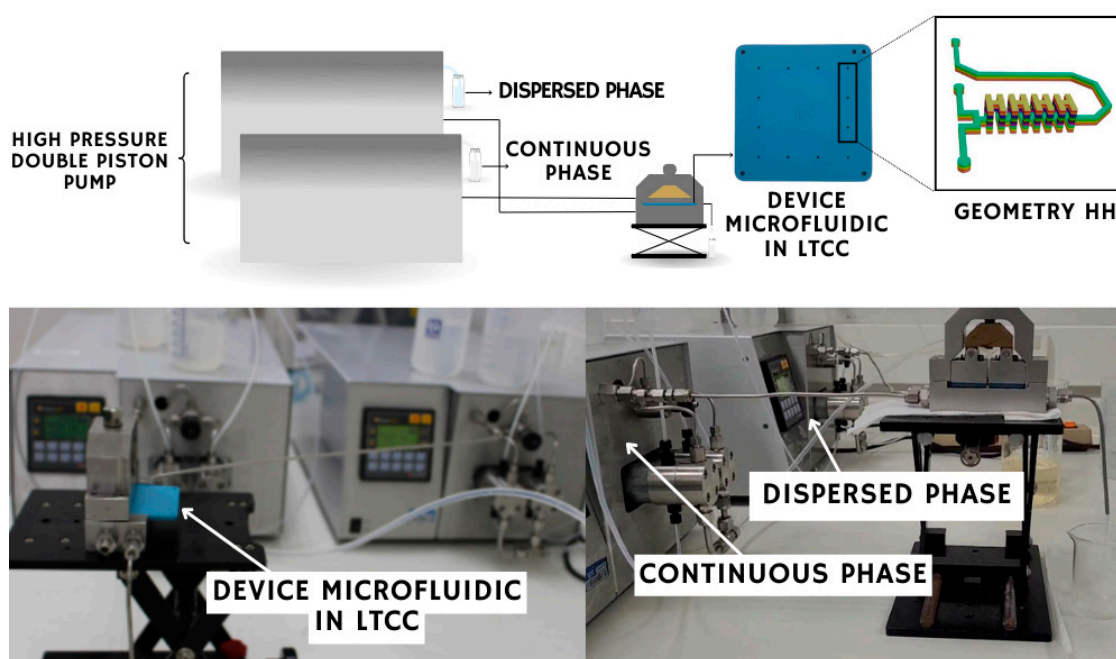
Figure 4. Layout of the microfluidic system and its components Sources: author herself.

2.3. Synthesis of Microparticles of PBCA

The formulation for the composition of the microcapsule synthesis emulsion was adapted from the methodologies [19,21,22], since the emulsion adopted was the water-in-oil one (W/O). The aqueous dispersed phase contained deionized water, ethyl alcohol, and the continuous oily phase contained caprylic/capric triglycerides, n-BCA, and Span 80 (which was tested in both phases), as described in Table 1.

Table 1. Description of formulation to produce emulsion containing microparticles of PBCA.

Ingredients	Function	Formulation				
		PBCA_MP_1	PBCA_MP_2	PBCA_MP_3	PBCA_MP_4	PBCA_MP_5
Caprylic/capric triglycerides	oil phase vehicle	31.7	42.2	48.7	61.9	73.4
n-butyl cyanoacrylate (n-BCA)	monomer	19.2	9.8	4.9	5.0	5.1
Span 80	emulsifier	0.7	0.8	0.8	0.8	0.8
Purified water	aqueous phase vehicle	26.4	36.0	40.4	27.4	15.4
Ethyl alcohol P.A.	initiator	22.0	11.3	5.1	5.0	5.1

Legend: proportion 45/55 (W/O): PBCA_MP_1; PBCA_MP_2 and PBCA_MP_3; proportion 30/70 (W/O): PBCA_MP_4 and proportion 20/80 (W/O): PBCA_MP_5.

Phase proportion was determined from an exploratory test of the formulation based on the literature, as well as the flow of both phases. The initial flow was 10 to 150 mL·min^{-1} [38–41].

2.4. Characterization of the Microcapsules

2.4.1. Dynamic Light Scattering (DLS)

Particle size and zeta potential of the PBCA microparticles was measured by dynamic light scattering (DLS), a technique which uses Nano Particle Analyzer—Particulate Systems. The disposable bucket with volume of ~0.9 mL was used to measure the size at the temperature of 25 °C and a backscattering angle of 165°. The sample amount was dispersed in water, centrifuged and the supernatants were analyzed in a triplicate method [13,42].

2.4.2. Particle Size Distribution

The size of the microparticles was measured by a laser beam diffraction technique using the Coulter LS230 equipment and the Beckman Coulter brand, MI, USA, specifically a Small Volume module. The samples were placed over an oily medium directly in the equipment. The values of the average volumetric diameter d(4.3) and the polydispersion of the polymeric microparticles was obtained after the accumulated reading and sequential recordings which lasted 60 s [43]. The value of the span distribution range was calculated using the (Equation (1)).

$$\text{Span} = ((\text{d90} - \text{d10}))/\text{d50} \tag{1}$$

Span distribution range. Legend: in which d90, d50 and d10 are corresponding to 90, 50 and 10% of the microparticles presented.

2.4.3. Scanning Electron Microscopy (SEM)

The morphology of the PBCA microparticle samples was evaluated by SEM-FEG, considering the FEI brand model Quanta 3D. The samples were dispersed in water, centrifuged for 20 min at 13,000 rpm, and deposited in aluminum stubs with carbon ribbon. Afterward, the samples were coated in gold/palladium (Au/Pd) for approximately 120 s and observed at an accelerating voltage of 20 kV [44].

2.4.4. Fourier Transformation Infrared Spectroscopy (FTIR)

FTIR spectra of n-BCA in TGCC and PBCA microparticles were recorded on a Nicolet iS50 FT-IR spectrometer (Thermo Scientific, WI, USA) with a resolution of 4 cm^{-1} in transmission mode. A total of 128 scans were recorded in the range of 4000 to 400 cm^{-1}. The sample was analyzed in liquid form after the process, without any dilution, washing, or centrifugation, and directly in the equipment accessory [17].

2.5. Statistical Analysis

The data were collected adopting a significance level of 5% (α = 0.05) and presented as mean and standard deviation (SD). The statistical analysis was performed using Minitab® statistical software (version 21.1.0) (PA, USA). To assess normality, the Kolmorov-Smirnov test was applied. The Two-tailed Student's *t*-test was used to compare paired results between two groups of parametric samples. The difference in effect between samples was evaluated by one-way analysis of variance (ANOVA) followed by post-test Tukey's test for multiple comparisons.

3. Results and Discussion

3.1. Influence of Channel Number in Micromixer

Previous studies have demonstrated the capability of producing emulsions and polymeric microparticles using microfluidic devices in LTCC. These studies utilized various ingredients and explored different total flow parameters to optimize the process [45,46]. However, the production mechanisms described in these reports, which involved forming polymers in their samples, differ from our investigation. Our study aimed to synthesize and produce PBCA microparticles within an emulsion.

In accordance with the work of Nimafar et al. and Kruss et al., microfluidic devices with 4, 10, and 15 channels were fabricated using LTCC to produce PBCA microparticles within an emulsion [36,37]. The parameters were initially tested in the micromixer with 4 channel sections, with total flow rates ranging from 10 to 150 mL·min^{-1}. The residence time was calculated based on the flow rates described in Table 2.

Table 2. Description of the test parameters in the microfluidic system.

Micromixer Geometry	Nº of Channels	Total Flow		Residence Time
		(mL·min^{-1})	(m³·s)	(s)
HH	4	10	1.67×10^{-7}	0.29
		25	4.17×10^{-7}	0.11
		50	8.33×10^{-7}	0.06
		70	1.17×10^{-6}	0.04
		100	1.67×10^{-6}	0.03
		150	2.50×10^{-6}	0.02
	10	53	8.91×10^{-7}	0.08
		75	1.25×10^{-6}	0.06
	15	39	6.50×10^{-7}	0.15
		78	1.30×10^{-6}	0.08
		109	1.82×10^{-6}	0.06

Samples were produced from the PBCA_MP_1 formulation in the 4-channel HH micromixer, and only those that remained stable after 24 h were collected at flow rates ranging from 25 to 150 mL·min^{-1}. These samples were aliquoted and centrifuged to separate their oily phases, and the supernatant was dispersed in water to analyze the

average diameter size of PBCA microparticles using DLS analysis. The results of the samples with total flow rates ranging from 25 to 150 mL·min^{-1} are illustrated in Figure 5.
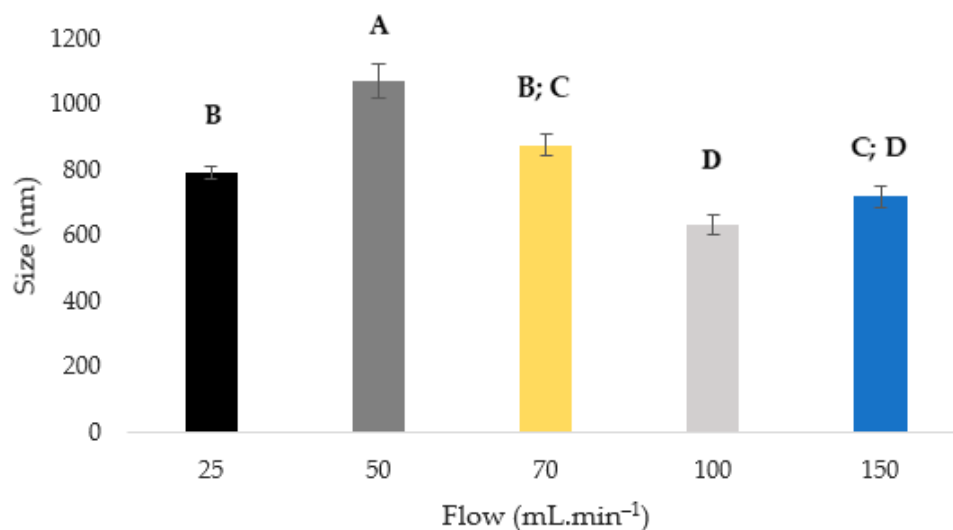

Figure 5. Diameter of PBCA microparticles in different flow rates using the HH micromixer with 4 channels. Legends: A, B, C and D representing letters in Statistical Analysis.

Statistically, the particle sizes shared similarities among 25 and 70; 70 and 150; and 100 and 150 mL·min^{-1}. Only at the flow rate of 50 mL·min^{-1} was possible to notice a significant difference in the average particle sizes among the samples. SEM images (Figure 6) revealed that microparticle agglomeration might occur depending on the collection flow rate. As demonstrated by the SEM photomicrographs, flow rates above 70 mL·min^{-1} did not exhibit microparticle agglomeration, indicating that the particles remained more dispersed under these conditions.

To evaluate the impact of the number of channels, versions of the HH micromixer containing 10 and 15 channels were tested using the same PBCA_MP_1 formulation. Adjustments to the flow rates were made considering the channel area, as shown in Table 2. The samples appeared uniform after 24 h of collection in both the 10-channel and 15-channel HH micromixers. DLS results indicated that, for a residence time of 0.08 s, the average particle size was 719.9 ± 33.64 nm in the 10-channel HH micromixer with a flow rate of 53 mL·min^{-1}, and 642.2 ± 4.0 nm in the 15-channel HH micromixer with a flow rate of 78 mL·min^{-1} (*p*-value 0.003). For a residence time of 0.06 s, the average particle size was 586.5 ± 11.31 nm in the 10-channel HH micromixer with a flow rate of 75 mL·min^{-1}, and 751.1 ± 5.57 nm in the 15-channel HH micromixer with a flow rate of 109 mL·min^{-1} (*p*-value 0.000).

These results suggest that the particles were smaller and more uniform in the 15-channel micromixer with a residence time of 0.08 s compared to the 10-channel micromixer with the same residence time. However, with a shorter residence time of 0.06 s, the 15-channel micromixer produced larger and more variable-sized particles than the 10-channel micromixer. This indicates that increasing the number of channels and adjusting the residence time significantly impacts the size and uniformity of the microparticles produced, as observed in the SEM images (Figure 7). This occurs since the residence time is related to the repetition of channel units; as the number of channels increases, the emulsion follows a longer path inside the mixer. This longer path enhances the mixing process and provides more time for the polymerization reaction to occur [24,47].
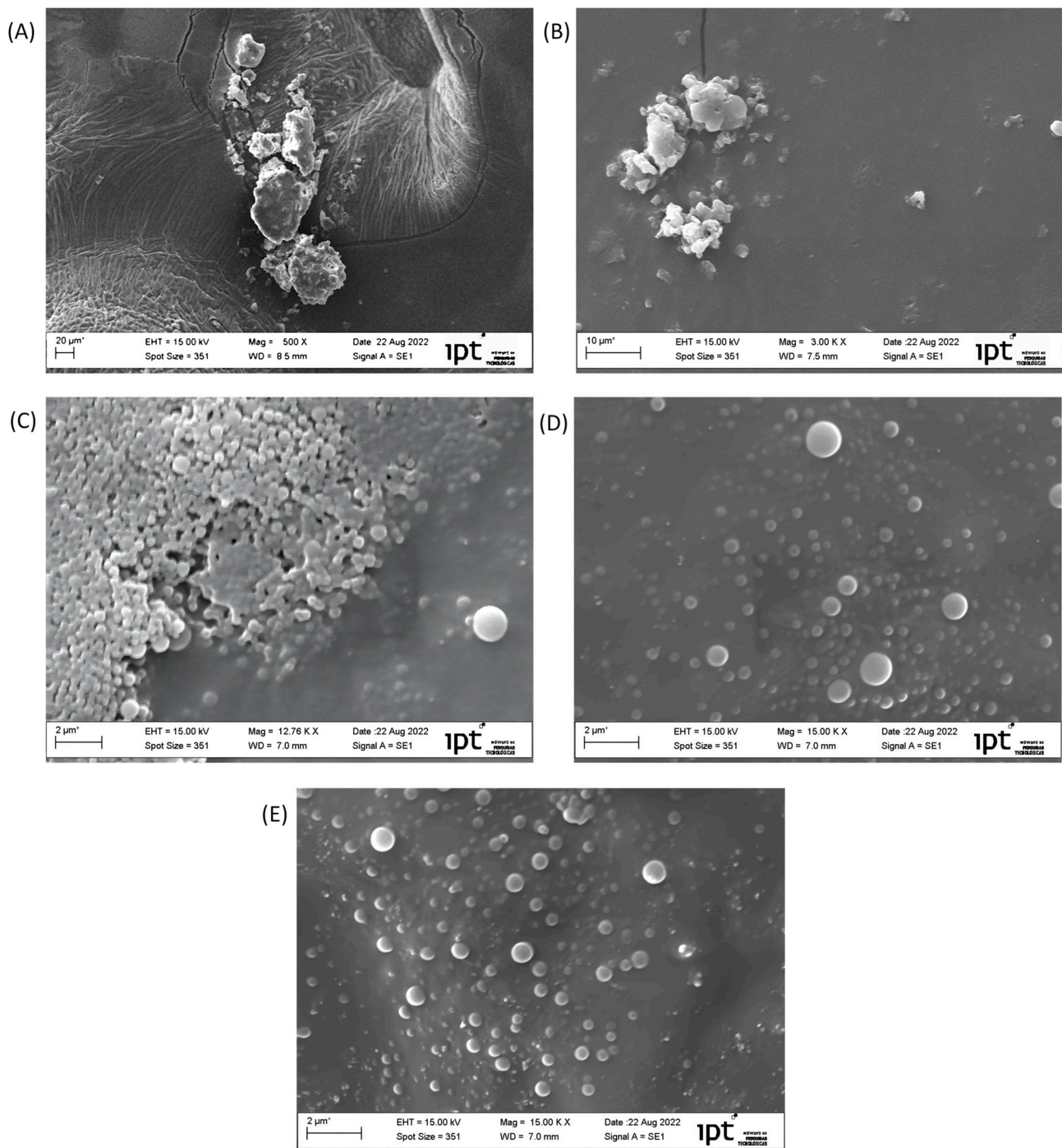
Figure 6. SEM photomicrographs of the sample PBCA_MP_1. Legend: (**A**). Sample collected in flow rate 25 mL·min^{-1}; (**B**). Sample collected in flow rate 50 mL·min^{-1}; (**C**). Sample collected in flow rate 70 mL·min^{-1}; (**D**). Sample collected in flow rate 100 mL·min^{-1}; and (**E**). Sample collected in flow rate 150 mL·min^{-1}. Magnitude 30.00 KX for samples of (**A**–**C**), and 15.00 KX for samples (**D**,**E**); (*) The asterisk indicates that the scale is in microns and has been rounded.
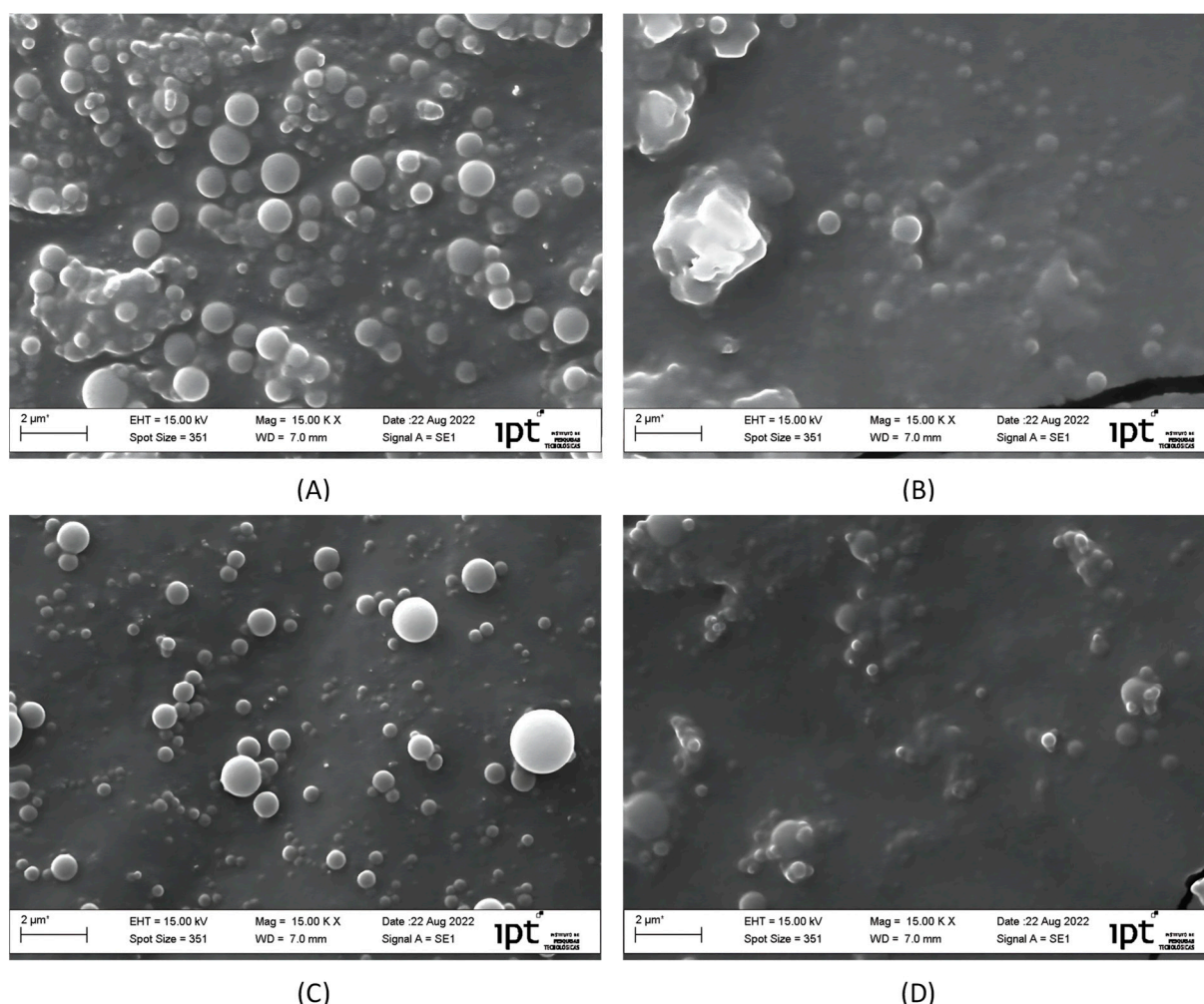
Figure 7. SEM photomicrographs of the sample PBCA_MP_1 collected in flow rates of 53, 75, 78 and 109 mL·min^{-1}. Legend: (**A**). Sample collected in flow rate 53 mL·min^{-1} and (**B**). Sample collected in flow rate 78 mL·min^{-1} with residence time of 0.08 s. (**C**). Sample collected in flow rate 75 mL·min^{-1} and (**D**). Sample collected in flow rate 109 mL·min^{-1} with a residence time of 0.06 s. Magnitude 15.00 KX; (*) The asterisk indicates that the scale is in microns and has been rounded.

3.2. Influence of Formulation Concentration Variation

Musyanovych and Landfester reported that different monomer concentrations affect the surface structure of capsules, with higher concentrations resulting in a thicker shell. Based on the previously mentioned study, various monomer concentrations were tested [21]. Additionally, it was considered that the emulsifier might cause uncontrolled polymerization by interacting with the monomer [22]. Therefore, it was decided to add the emulsifier into the aqueous phase. Micelles act at the interface of emulsion phases, serving as a point of connection between the monomer in the oil phase and the initiator in the aqueous phase. Sorbitan monooleate, a non-ionic emulsifier with a hydrophilic-lipophilic balance (HLB) of 4, was chosen as it is suitable for oil-in-water emulsions [22,48]. Thus, samples PBCA_MP_2 and PBCA_MP_3 were tested in the flow rate of 78 mL·min^{-1} in the 15-channel HH micromixer, which, as described in the previous section, presented a more homogeneous particle diameter, being the emulsifier added into the aqueous phase.

PBCA_MP_2 exhibited phase separation after collection, dividing into three distinct parts: oil in the upper phase, emulsion in the middle, and water at the bottom of the vial. The same phenomenon was observed for PBCA_MP_3. However, after 24 h, these samples developed a suspended and flocculated appearance, indicating that the reaction still occurred despite the lack of homogeneous emulsion formation. This instability may

be attributed to the change in emulsifier addition from the oil phase to the aqueous phase. The emulsifier concentration may have been insufficient to stabilize the emulsion, as noted in previous studies [22,48]. Despite varying concentrations and maintaining the emulsifier in the same phase, stability was not achieved.

At another total flow rate, 39 mL·min^{-1}, the same sample conditions were evaluated with a residence time of 0.15 s. Both samples were homogeneous upon collection, and after 24 h, they did not show phase separation as observed at the flow rate of 78 mL·min^{-1}. However, it was noted that the samples coalesced, indicating that the emulsifier in the aqueous phase was still insufficient to maintain the stability of the emulsion and the formation of microparticles. Under these process conditions, the residence time minimized phase separation, but it was not enough to prevent sample coalescence.

The monomer concentration promotes an increase in encapsulation efficiency but a decrease in the concentration of the encapsulated substance. For cosmetic applications, studies have typically not employed high concentrations of n-BCA [17,21,49]. Therefore, assays were conducted using 5% (*w/w*) of n-BCA, with a flow rate of 39 mL·min^{-1}, which allowed the collection of homogeneous samples. Thus, for process and formulation parameters, a strategy was adopted to adjust the proportion between the continuous and dispersed phases of the emulsion. This involved expanding the range of the continuous phase proportion and reducing the dispersed phase to enhance the interaction of the emulsifier with the oily phase, which has a greater affinity for the emulsifier's structure [50]. This was done while maintaining the initiator-to-monomer ratio and the emulsifier concentration, which could affect the polymerization reaction rate, as previously mentioned.

3.3. Influence of Phase Proportion

Formulations PBCA_MP_4 and PBCA_MP_5 were tested with varying phase proportions. PBCA_MP_4 showed slight phase separation at the bottom of the vial after 24 h. The particle size was analyzed using Coulter in an oily medium, as the samples did not exhibit sufficient stability in water for DLS analysis. The average particle diameter was 48.87 ± 5.63 μm with a span of 1.94. When observed under SEM (Figure 8), these samples exhibited aggregation, which hindered a clearer visualization of the particle formation.
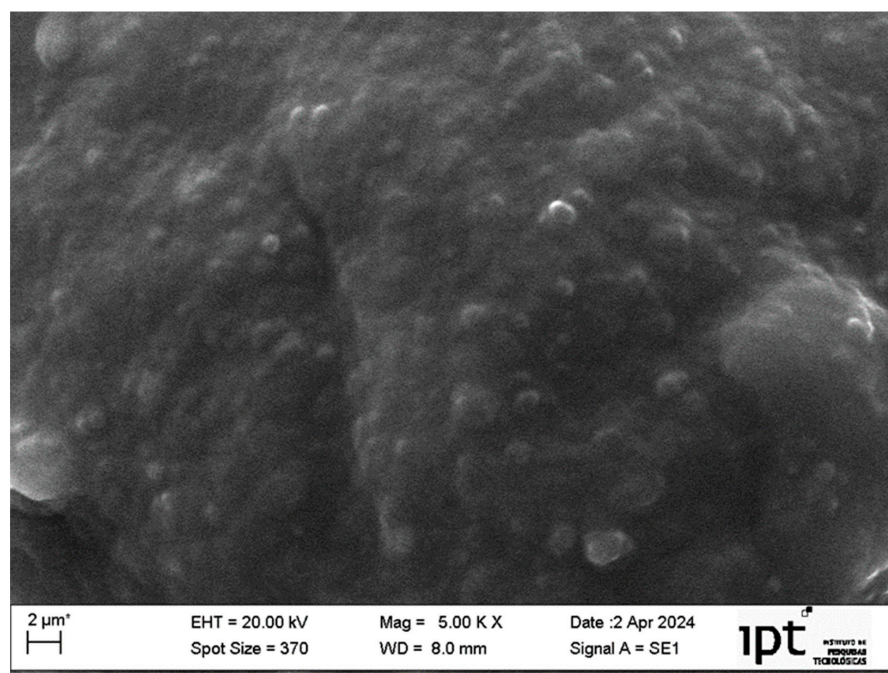
Figure 8. SEM photomicrograph of the sample PBCA_MP_4 collected in the flow rate of 39 mL·min^{-1} with phase proportion of 30/70 (W/O). Legend: Magnitude 5.00 KX; (*) The asterisk indicates that the scale is in microns and has been rounded.

Sample PBCA_MP_5 exhibited homogeneity without phase separation after 24 h. This experiment was analyzed using a laser diffraction particle size analysis and showed particle size of 74.73 ± 17.3 μm with span of 2.77. In Figure 9, the formation of the microparticles was more visible compared to the previous sample, although aggregation was still present. The perspective from this result suggests that by reducing the emulsifier concentration in the aqueous phase and increasing it in the oily phase, the hydrophobic nature of the surfactant facilitates stable emulsion formation, even after 24 h. However, these samples continued to exhibit a higher amount of surfactant, likely contributing to the observed aggregation.
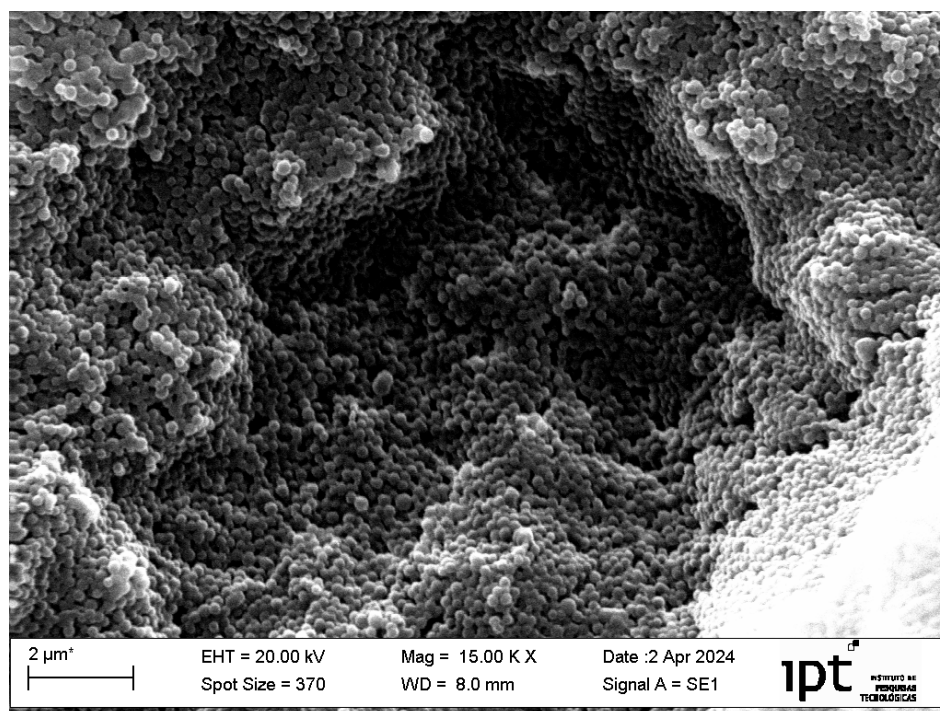
Figure 9. SEM photomicrograph of the sample PBCA_MP_5 collected at the flow rate of 39 mL·min^{-1}. Legend: Sample with magnitude 15.00 KX; (*) The asterisk indicates that the scale is in microns and has been rounded.

Despite variations in formation, statistically, there was no difference in the size obtained for PBCA_MP_4 and PBCA_MP_5 (*p*-value 0.364). This suggested that the formulation influenced the formation, maintaining consistent size profiles delivered by the micromixer. In contrast to other methodologies aimed at producing nanocapsules or nanoparticles, the present methodology utilized emulsion polymerization in a microfluidic system for microparticle production. Other methodologies often employ different approaches to achieve controlled polymerization of n-BCA. Additionally, these methods typically involve multiple preparation steps such as emulsion, mini-emulsion, evaporation, washing, and purification, with synthesis times extending beyond 24 h in some cases [13,21,49,51].

3.4. FTIR

Fourier transform infrared spectroscopy (FTIR) was employed to characterize the formation of PBCA via anionic polymerization, focusing on the absorption of specific frequencies that reflect the chemical structures involved. Pure monomer was added to TGCC in a 1:1 ratio to identify peaks indicating polymerization in the synthesized samples. However, it was observed that indicative peaks of polymer formation were also present in the monomer-oil sample alone. This occurrence suggests the possibility of pre-polymerization or polymerization initiation within the monomer-oil phase before the intended synthesis process [52]. The presence of polymer formation peaks in the monomer-oil sample suggests

that n-BCA undergoes self-polymerization, resulting in the formation of a high molecular weight polymer. Subsequently, depolymerization may occur, followed by the production of a polymer with a lower molecular weight. This observation indicates a complex polymerization behavior of n-BCA, possibly influenced by conditions such as temperature, presence of initiators, or other factors affecting polymerization kinetics and outcomes. In the PBCA_MP_1 samples collected from the 4- and 10-channel HH micromixers, absorption peaks were observed at specific wavelengths: peaks around 3378 cm^{-1} indicate vibrations of the –OH groups; peaks around 1750 cm^{-1} correspond to carbonyl (C=O) groups; the absorption peak at approximately 2238 cm^{-1} corresponds to the nitrile (C≡N) group [53].

In Figure 10, the samples collected from the 15-channel HH micromixer have shown the same peaks corresponding to the formation of PBCA microparticles for all PBCA_MP_1 and PBCA_MP_5 samples, when compared to the corresponding peaks of hydroxyl, carbonyl, and nitrile groups.
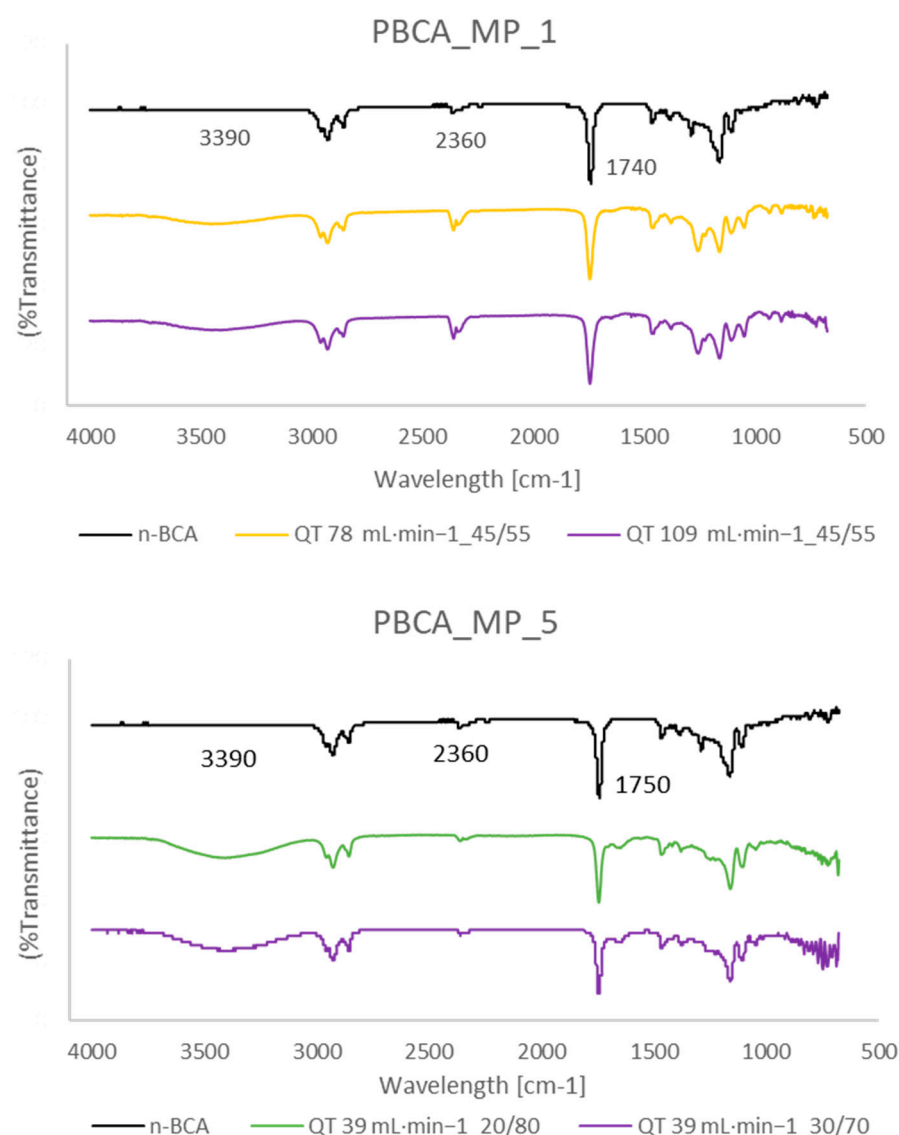
Figure 10. Spectrum of the PBCA_MP_1 and PBCA_MP_5 samples collected in different flow rates in the 15-channel micromixer.

4. Conclusions

PBCA microparticles were synthesized via anionic emulsion polymerization (W/O) using a microfluidic system, accomplished in a single step. The microfluidic device, featuring a 15-channel HH geometry, was fabricated and proved effective for microparticle

production. Optimal results for PBCA microparticle formation were achieved with total flow rates of 39 and 78 mL·min^{-1}. The addition of ethanol in a 1:1 ratio with the initiator facilitated the interfacial anionic polymerization reaction. Span 80 contributed to the stability of the microparticle suspension, with phase ratios of 45/55 (W/O) for samples containing 19.2% (*w/w*) n-BCA and 20/80 (W/O) for samples containing 5.0% (*w/w*) n-BCA. The microparticles exhibited a spherical shape in SEM photomicrographs, with average diameters of 642 nm in DLS analysis and 74.73 μm in laser diffraction particle size analysis. FTIR analyses confirmed their composition as PBCA polymer.

Based on these results, there is a need to explore other emulsifiers, both hydrophilic and lipophilic, for use in both continuous and dispersed phases. This exploration aims to enhance the homogeneity of microparticle diameters. Furthermore, it is crucial to optimize monomer concentrations based on the active ingredients used and the intended applications of the microparticles. A significant challenge in this process lies in adjusting the residence time relative to the flow rate to achieve uniform microparticle sizes. This optimization is essential for ensuring consistent quality and performance in various applications.

References

1. Casanova, F.; Santos, L. Encapsulation of Cosmetic Active Ingredients for Topical Application—A Review. *J. Microencapsul.* **2016**, *33*, 1–17. [CrossRef]
2. Kouassi, M.C.; Grisel, M.; Gore, E. Multifunctional Active Ingredient-Based Delivery Systems for Skincare Formulations: A Review. *Colloids Surf. B Biointerfaces* **2022**, *217*, 112676. [CrossRef]
3. Parente, J.F.; Sousa, V.I.; Marques, J.F.; Forte, M.A.; Tavares, C.J. Biodegradable Polymers for Microencapsulation Systems. *Adv. Polym. Technol.* **2022**, *2022*, 4640379. [CrossRef]
4. Zhang, F.; Fan, J.B.; Wang, S. Interfacial Polymerization: From Chemistry to Functional Materials. *Angew. Chem. Int. Ed.* **2020**, *59*, 21840–21856. [CrossRef]
5. El-Damrawi, G.; Hassan, A.K.; Meikhail, M.S. *Principles of Polymerization*; Wiley: Hoboken, NJ, USA, 1996; Volume 37, ISBN 3175723993.
6. El-hoshoudy, A.N.M.B. Emulsion Polymerization Mechanism. In *Recent Research in Polymerization*; InTech: Houston, TX, USA, 2018.
7. Landfester, K.; Musyanovych, A.; Mailänder, V. From Polymeric Particles to Multifunctional Nanocapsules for Biomedical Applications Using the Miniemulsion Process. *J. Polym. Sci. Part A Polym. Chem.* **2010**, *48*, 493–515. [CrossRef]
8. Musyanovych, A.; Landfester, K. Polymer Micro- and Nanocapsules as Biological Carriers with Multifunctional Properties. *Macromol. Biosci.* **2014**, *14*, 458–477. [CrossRef]

9.   Soni, D.; Trivedi, M.; Ameta, R. *Microwave-Assisted Organic Synthesis*; Ameta, S.C., Punjabi, P.B., Ameta, R., Ameta, C., Eds.; Apple Academic Press: Burlington, ON, Canada, 2014; ISBN 9781482254242.

10.   Mills, N.; Jenkins, M.; Kukureka, S. Molecular Structures and Polymer Manufacture. In *Plastics: Microstructure and Engineering Applications*; Elsevier: Amsterdam, The Netherlands, 2020; pp. 13–31. [CrossRef]

11.   Margerison, D.; East, G.C. *Ionic Polymerization*; Elsevier Inc.: Amsterdam, The Netherlands, 1967; ISBN 9780124095472.

12.   Hansali, F.; Poisson, G.; Wu, M.; Bendedouch, D.; Marie, E. Miniemulsion Polymerizations of N-Butyl Cyanoacrylate via Two Routes: Towards a Control of Particle Degradation. *Colloids Surf. B Biointerfaces* **2011**, *88*, 332–338. [CrossRef]

13.   Bagad, M.; Khan, Z.A. Poly(n-Butylcyanoacrylate) Nanoparticles for Oral Delivery of Quercetin: Preparation, Characterization, and Pharmacokinetics and Biodistribution Studies in Wistar Rats. *Int. J. Nanomed.* **2015**, *10*, 3921–3935. [CrossRef]

14.   Elzayat, A.; Adam-Cervera, I.; Álvarez-Bermúdez, O.; Muñoz-Espí, R. Nanoemulsions for Synthesis of Biomedical Nanocarriers. *Colloids Surf. B Biointerfaces* **2021**, *203*, 111764. [CrossRef]

15.   Gao, S.; Xu, Y.; Asghar, S.; Chen, M.; Zou, L.; Eltayeb, S.; Huo, M.; Ping, Q.; Xiao, Y. Polybutylcyanoacrylate Nanocarriers as Promising Targeted Drug Delivery Systems. *J. Drug Target.* **2015**, *23*, 481–496. [CrossRef]

16.   Tomcin, S.; Baier, G.; Landfester, K.; Mailänder, V. Pharmacokinetics on a Microscale: Visualizing Cy5-Labeled Oligonucleotide Release from Poly(n-Butylcyanoacrylate) Nanocapsules in Cells. *Int. J. Nanomed.* **2014**, *9*, 5471–5489. [CrossRef]

17.   Duan, J.; Mansour, H.M.; Zhang, Y.; Deng, X.; Chen, Y.; Wang, J.; Pan, Y.; Zhao, J. Reversion of Multidrug Resistance by Co-Encapsulation of Doxorubicin and Curcumin in Chitosan/Poly(Butyl Cyanoacrylate) Nanoparticles. *Int. J. Pharm.* **2012**, *426*, 193–201. [CrossRef]

18.   Limouzin, C.; Caviggia, A.; Ganachaud, F.; Hémery, P. Anionic Polymerization of N-Butyl Cyanoacrylate in Emulsion and Miniemulsion. *Macromolecules* **2003**, *36*, 667–674. [CrossRef]

19.   Al Khouri Fallouh, N.; Roblot-Treupel, L.; Fessi, H.; Devissaguet, J.P.; Puisieux, F. Development of a New Process for the Manufacture of Polyisobutylcyanoacrylate Nanocapsules. *Int. J. Pharm.* **1986**, *28*, 125–132. [CrossRef]

20.   Weiss, C.K.; Ziener, U.; Landfester, K. A Route to Nonfunctionalized and Functionalized Poly (n-Butylcyanoacrylate) Nanoparticles: Preparation in Miniemulsion. *Macromolecules* **2007**, *40*, 928–938. [CrossRef]

21.   Musyanovych, A.; Landfester, K. Synthesis of Poly(Butylcyanoacrylate) Nanocapsules by Interfacial Polymerization in Miniemulsions for the Delivery of DNA Molecules. In *Surface and Interfacial Forces—From Fundamentals to Applications*; Springer: Berlin/Heidelberg, Germany, 2007; Volume 134, pp. 120–127. ISBN 9783540680185.

22.   Hansali, F.; Wu, M.; Bendedouch, D.; Marie, E. N-Butyl Cyanoacrylate Miniemulsion Polymerization via the Phase Inversion Composition Method. *Colloids Surf. A Physicochem. Eng. Asp.* **2012**, *393*, 133–138. [CrossRef]

23.   Hardt, S.; Schönfeld, F. *Microfluidic Technologies for Miniaturized Analysis Systems*; Springer Science & Business Media: Berlin, Germany, 2007; ISBN 9780387285979.

24.   Cheng, J.; Deming, T.J. Micromixing Within Microfluidic Devices. *Pept. Mater.* **2011**, *310*, 1–26. [CrossRef]

25.   Kang, H.; Zhu, Y.; Shen, J.; Yang, X.; Chen, C.; Cao, H.; Li, C. Preparation of Silica-Sustained Electrospun Polyvinylpyrrolidone Fibers with Uniform Mesopores via Oxidative Removal of Template Molecules by H_2O_2 Treatment. *Mater. Res. Bull.* **2010**, *45*, 830–837. [CrossRef]

26.   Kulkarni, M.B.; Goel, S. Microfluidic Devices for Synthesizing Nanomaterials—A Review. *Nano Express* **2020**, *1*, 032004. [CrossRef]

27.   Cai, G.; Xue, L.; Zhang, H.; Lin, J. A Review on Micromixers. *Micromachines* **2017**, *8*, 274. [CrossRef]

28.   Shen, J.; Shafiq, M.; Ma, M.; Chen, H. Synthesis and Surface Engineering of Inorganic Nanomaterials Based on Microfluidic Technology. *Nanomaterials* **2020**, *10*, 1177. [CrossRef]

29.   Alrifaiy, A.; Lindahl, O.A.; Ramser, K. Polymer-Based Microfluidic Devices for Pharmacy, Biology and Tissue Engineering. *Polymers* **2012**, *4*, 1349–1398. [CrossRef]

30.   Raza, W.; Hossain, S.; Kim, K.Y. A Review of Passive Micromixers with a Comparative Analysis. *Micromachines* **2020**, *11*, 455. [CrossRef]

31.   Gomez, H.C.; Cardoso, R.M.; de Novais Schianti, J.; de Oliveira, A.M.; Gongora-Rubio, M.R. Fab on a Package: LTCC Microfluidic Devices Applied to Chemical Process Miniaturization. *Micromachines* **2018**, *9*, 285. [CrossRef]

32.   Valencia, P.M.; Pridgen, E.M.; Rhee, M.; Langer, R.; Farokhzad, O.C.; Karnik, R. Microfluidic Platform for Combinatorial Synthesis and Optimization of Targeted Nanoparticles for Cancer Therapy. *ACS Nano* **2013**, *7*, 10671–10680. [CrossRef]

33.   Zhang, L.; Chen, Q.; Ma, Y.; Sun, J. Microfluidic Methods for Fabrication and Engineering of Nanoparticle Drug Delivery Systems. *ACS Appl. Bio Mater.* **2020**, *3*, 107–120. [CrossRef]

34.   Ribeiro-costa, R.M.; Rodrigues, M.; Gongora-rubio, M.R.; Michaluart-júnior, P.; Ré, M.I. Preparation of Protein-Loaded-PLGA Microspheres by an Emulsion/Solvent Evaporation Process Employing LTCC Micromixers. *Powder Technol.* **2009**, *190*, 107–111. [CrossRef]

35.   Malecha, K.; Dawgul, M.; Pijanowska, D.G.; Golonka, L.J. LTCC Microfluidic Systems for Biochemical Diagnosis. *Biocybern. Biomed. Eng.* **2011**, *31*, 31–41. [CrossRef]

36.   Nimafar, M.; Viktorov, V.; Martinelli, M. Experimental Comparative Mixing Performance of Passive Micromixers with H-Shaped Sub-Channels. *Chem. Eng. Sci.* **2012**, *76*, 37–44. [CrossRef]

37.   Kruss, W.C.; Lucia, M.; Bejarano, M.; Ferreira, K.; Cruz, D.N.; Lima, A.P.; Lanigra, K. *LTCC 3D Passive Micromixers to Oil in Water Emulsion Scale-Up*; Instituto de Pesquisas Tecnológicas: São Paulo, Brazil, 2019.

38. Mae, K.; Maki, T.; Hasegawa, I.; Eto, U.; Mizutani, Y.; Honda, N. Development of a New Micromixer Based on Split/Recombination for Mass Production and Its Application to Soap Free Emulsifier. *Chem. Eng. J.* **2004**, *101*, 31–38. [CrossRef]
39. Matsuyama, K.; Mine, K.; Kubo, H.; Mae, K. Design of Micromixer for Emulsification and Application to Conventional Commercial Plant for Cosmetic. *Chem. Eng. J.* **2011**, *167*, 727–733. [CrossRef]
40. Makgwane, P.R.; Ray, S.S. Synthesis of Nanomaterials by Continuous-Flow Microfluidics: A Review. *J. Nanosci. Nanotechnol.* **2014**, *14*, 1338–1363. [CrossRef]
41. Gomez, H.C.; Agio, B.O.; Da Silva, J.G.; Pereira Cerize, N.N.; De Oliveira, A.M.; Guimaraes, K.L.; Da Cunha, M.R.; Seabra, A.C.; Gongora-Rubio, M.R. LTCC 3D Micromixers for Non-Miscible Fluids Microemulsion Generation. In Proceedings of the IMAPS/ACerS 12th International Conference and Exhibition on Ceramic Interconnect and Ceramic Microsystems Technologies, CICMT 2016, Ventura, CA, USA, 17–20 January 2016; pp. 96–102. [CrossRef]
42. Srikar, G.; Rani, A.P. Study on Influence of Polymer and Surfactant on in Vitro Performance of Biodegradable Aqueous-Core Nanocapsules of Tenofovirdisoproxil Fumarate by Response Surface Methodology. *Braz. J. Pharm. Sci.* **2019**, *55*, e18736. [CrossRef]
43. Betz, M.; Kulozik, U. Microencapsulation of Bioactive Bilberry Anthocyanins by Means of Whey Protein Gels. *Procedia Food Sci.* **2011**, *1*, 2047–2056. [CrossRef]
44. Rashidinejad, A.; Loveday, S.M.; Jameson, G.B.; Hindmarsh, J.P.; Singh, H. Rutin-Casein Co-Precipitates as Potential Delivery Vehicles for Flavonoid Rutin. *Food Hydrocoll.* **2019**, *96*, 451–462. [CrossRef]
45. de Novais Schianti, J. Sistemas Microfluídicos Aplicados Na Produção de Micro e Nanopartículas. Ph.D. Thesis, Universidade de São Paulo: São Paulo, Brazil, 2012.
46. Cobas Gomez, H. Sistemas Microfluídicos Cerâmicos Para Miniaturização de Processos Químicos Aplicados à Fabricação de Nanopartículas. Ph.D. Thesis, Universidade de São Paulo: São Paulo, Brazil, 2016.
47. Tran-Minh, N.; Dong, T.; Karlsen, F. An Efficient Passive Planar Micromixer with Ellipse-like Micropillars for Continuous Mixing of Human Blood. *Comput. Methods Programs Biomed.* **2014**, *117*, 20–29. [CrossRef]
48. Ng, N.; Rogers, M.A. Surfactants. In *Encyclopedia of Food Chemistry*; Elsevier: Amsterdam, The Netherlands, 2019; Volume 1, pp. 276–282. ISBN 9780128140451.
49. Lin, M.H.C.; Lai, P.S.; Chang, L.C.; Huang, W.C.; Lee, M.H.; Chen, K.T.; Chung, C.Y.; Yang, J.T. Characterization and Optimization of Chitosan-Coated Polybutylcyanoacrylate Nanoparticles for the Transfection-Guided Neural Differentiation of Mouse Induced Pluripotent Stem Cells. *Int. J. Mol. Sci.* **2021**, *22*, 8741. [CrossRef]
50. Farn, R.J. *Chemistry and Technology of Surfactants*; Wiley: Hoboken, NJ, USA, 2007; ISBN 1405126965.
51. Yordanov, G.G.; Dushkin, C.D. Preparation of Poly(Butylcyanoacrylate) Drug Carriers by Nanoprecipitation Using a Pre-Synthesized Polymer and Different Colloidal Stabilizers. *Colloid Polym. Sci.* **2010**, *288*, 1019–1026. [CrossRef]
52. Keller, B.L.; Lohmann, C.A.; Kyeremateng, S.O.; Fricker, G. Synthesis and Characterization of Biodegradable Poly(Butyl Cyanoacrylate) for Drug Delivery Applications. *Polymers* **2022**, *14*, 998. [CrossRef]
53. Hu, J.; Xiao, Z.; Zhou, R.; Li, Z.; Wang, M.; Ma, S. Synthesis and Characterization of Polybutylcyanoacrylate-Encapsulated Rose Fragrance Nanocapsule. *Flavour Fragr. J.* **2011**, *26*, 162–173. [CrossRef]